ORIGINAL PAPER

RESEARCH USING ATOMIC METHODS ON MATERIALS USED IN THE MANUFACTURE OF COMPONENTS FOR MEDICAL IMPLANTS

VERONICA DESPA[1], FLORINA VIOLETA ANGHELINA[1]*, DORIN IANCU[2], CARMEN OTILIA RUSANESCU[3]

Manuscript received: 03.09.2017; Accepted paper: 11.10.2017;
Published online: 30.12.2017.

Abstract. *The materials used to manufacture prosthetic components must meet the conditions of biocompatibility imposed by the human body, to be mechanically resistant, to present a good resistance to corrosion, to be resistant to aging process and not to generate flows of attrition particles. This paper aims the selection and analising of some biocompatible metallic materials (the austenitic stainless steel and titanium alloys). Thus, various prosthetic elements made by rapid prototyping (RP) technologies from Ti6Al4V alloys obtained using laser selective melting (SLS Technology) have a major advantage in the special geometric form for medicine, creating a personalized implant for each patient and with superior properties on the quality of the material used. Studies in recent years have led to the conclusion that the biocompatibility of an implant depends on many factors such as: the general health status of the patient, age, tissue permeability, immunological factors, but also the implant characteristics (roughness and porosity of the material, chemical composition, corrosion properties, toxicity, etc.). For this reason, samples of 316L stainless steel and Ti6Al4V titanium alloy were analyzed.*

Keywords: *stainless steel 316L, Ti6Al4V alloy, Selective laser sintering (SLS)*

1. INTRODUCTION

Recently, biomaterials research has been developed and intensified, especially due to an increased demand for personalized prostheses made of bioactive materials, based on the particularities of each individual. The basic structure of biocompatible prostheses is the subject of research and study of many researches in the field. The success of a biomaterial or an implant is highly dependent on three major factors (i) the properties (mechanical, chemical and tribological) of the biomaterial in question (ii) biocompatibility of the implant and (iii) the health condition of the recipient and the competency of the surgeon. Especially after the world wars, the need for biomaterials was acutely felt and in the recent context of global terrorism, this field assumes much more significance [1, 32-34].

The commonly used surgical implants are usually made from one of the three types of materials: austenitic stainless steel, cobalt-chromium alloy, and titanium and its alloys and out of these, 316L austenitic stainless steel is the most commonly used implant material as it is

[1] Valahia University of Targoviste, Faculty of Materials Engineering and Mechanics, 130004 Targoviste, Romania. E-mail (*Corresponding author): vianghelina@yahoo.com; dumiver@yahoo.com.
[2] Valahia University of Targoviste, Faculty of Economics, 130004 Targoviste, Romania. E-mail: dorin_iancu04@yahoo.com.
[3] Politehnica University of Bucharest, 060042 Bucharest, Romania. E-mail: otiliarusanescu@yahoo.com.

cost effective [2]. The 316L stainless steel it was one of the materials selected for this experimental study.

The 316L stainless steel it used to make prosthetic fixation pins, oral implants (screws and nuts), cardiovascular implants (stent device), modular hip implants, etc. and this metallic material was chosen because of her attractive properties: excellent corrosion resistance, good mechanical properties, adequate biocompatibility, remarkable plasticity and a very good cost-effectiveness. Also, the 316L stainless steel are the most commonly used materials for coronary stents. Stents are thin-wire scaffold structures used in angioplasty for the treatment of atherosclerosis, and are permanently implanted into the body [3]. Since the interface between the host tissue and stent material plays an important role in stent biocompatibility, most advances in stent design have been focused on modifying the surface properties, including the surface finish [4]. Other studies [5, 6] have shown that the constitution and surface characteristics of the material may determine the nature of the host response and the long-term stent patency rate.The chemical composition of the stent surface is dictated by the final processing steps during manufacture, and the rate of chemical and electrochemical reactions, that may later occur, is strongly dependent upon the properties of the passive layer formed on the stent surface. Under certain circumstances, the passivation layer can be broken down, and corrosion and consequently corrosion fatigue can occur, resulting in failure [5].

For medical devices, biological complications associated are a common problem for prosthetic fixation systems fabricated from stainless steel, in this case the percentage of infection ranging from 2% to 30% [7]. Thus, the infections caused by the use of stainless steel pins, stents, as well as other devices can be partially avoided by replacing this material with Ti6Al4V titanium alloy. The 316L stainless steel for implants can present the phenomenon of localized corrosion, caused by the condition of the surface (surface quality, roughness etc.) and metallurgical parameters [2, 8-10, 35]. But, the infuence of the metallurgical parameters could not be separated from a possible chemical compositional effect. Localized corrosion attacks and leaching of metallic ions from implants necessitate improvement in the corrosion resistance of the currently used type 316L by bulk alloying or modifying the surface [2, 11].

The Ti6Al4V alloy type selected for this study was done by selective laser sintering technology and is heavily used in the realization the current implantable devices. This alloy has good properties of durability, flexibility, light weight and corrosion resistance [12, 13]. The modulus of elasticity of titanium based alloys is much lower and closer to that of the bone when compared to 316L and Co-Cr alloys and hence they are more preferred for long term applications. As of now, they are used as implants for joint replacements, bone fixation, dental implants, heart pacemakers, artificial heart valves, stents and components in high-speed blood centrifuges because of their high specific strength and chemical stability [14, 15]. Titanium and Ti6Al4V present low shear strength and low wear resistance when used in an orthopedic prosthesis. Also important is the mismatch of Young's modulus between the titanium implant (103–120 GPa) and bone (10–30 GPa), which is unfavorable for bone healing and remodeling [16]. Fatigue corrosion resistance of titanium is almost independent of the pH value while the fatigue corrosion strength of stainless steel starts decreasing below a pH value of 4. Thus the corrosion resistance of the passive film is very much dependent on the thickness of the layer formed and the nature of the elements present in titanium and its alloys [17]. However, the nature and distribution of corrosion products released into the body from these orthopedics implants remains, still as an important issue [18]. Hence, currently many researchers are working on the enhancement on the improvement of surface properties of titanium based alloys [11, 17].

Laser processing also is now being used in implant applications to produce a high degree of purity with enough roughness for good osseointegration [19]. Yue et al. used the

exciter laser to modify the surface of the Ti6Al4V alloy to improve its corrosion resistance and there was a seven fold increase in the corrosion resistance [20].

Surface modifications are often performed on the biomedical implants to improve corrosion resistance, wear resistance, surface texture and biocompatibility [21-24]. All the modified surfaces should be tested for its corrosion behavior invariably apart from improving other desired properties. The effect of corrosion is among the major causes of failure of metal implants. In addition, corrosion fatigue and fretting corrosion have also been observed in bone plates and screws at the bone-stem, and stem-cement interfaces of modular hip implants [25]. The failure of stent device due to stress corrosion fatigue is a long term problem and this failure has been attributed to the weak surface of the implant [26]. This stress corrosion cracking in biomedical implants can lead to loss of structural integrity of the implanted device and its functions. Thus these complications lead to disintegration of the implant [27].

It has been found that this dissolution of metal ions can be reduced by suitable biocompatible inorganic coatings, such as hydroxyl-apatite (HAP) coating with some binders, and this can lead to delay in corrosion and wear and also minimize the loosening of implants from bone [28-30]. Thus the only solution to impede corrosion is by choosing better quality materials with appropriate coating [29, 36-40].

2. MATERIALS AND METHODS

Investigations were performed on a representative 316L stainless steel sample i.e. batches of 316 L steel bars developed within a national PNCDI project. In order to assess the compliance of the bars with Φ 35, three samples (C, D, E) (see Fig. 1.a) taken from the batch bars were tested. Along with the spectrochimically investigated 316 L steel samples (see Fig.1b), two types of drawn bars (Φ=10mm and Φ=6mm) were tested spectrochimically. A special clamping device was used to investigate these bars. OES-ASE spectrometry (optical emission spectrometry using Arc / Spark excitation) tests were made with a Foundry-Master spectrometer having the following characteristics: Paschen-Runge optic with 140-500 nm wavelength range; spark discharge source of 500 V at 450 Hz rate; Ar purged stand; tungsten counter-electrod washed with argon; evacuated optics.

Figure 1a). The samples C, D, E.

Figure 1b). The steel samples spectrochimically investigated.

The results of the spectral tests of samples are presented in additionals data are given in Figs. 2 and 3, and Table 1. It was chosen one sample from the spectrochimically investigated 316 L steel samples who was investigated by metallographic optical microscopy and SEM-EDS microscopy (Scanning Electron Microscopy & Energy Dispersion Spectroscopy). This sample has 4 distinct sparks, which are representative of the sparking process.

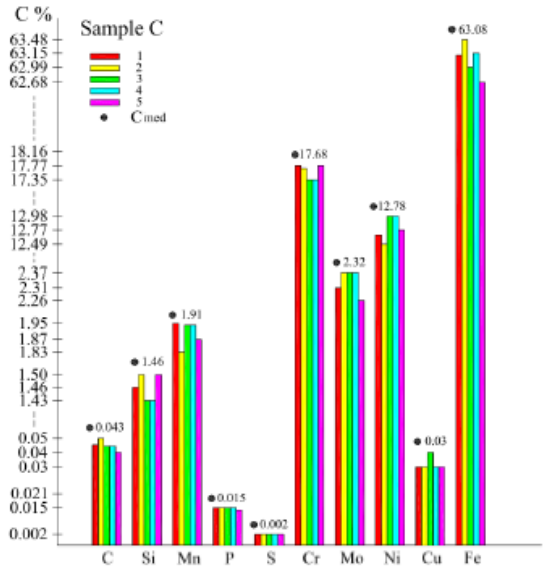

Figure 2. The concentration values and the average concentration associated with sample C.

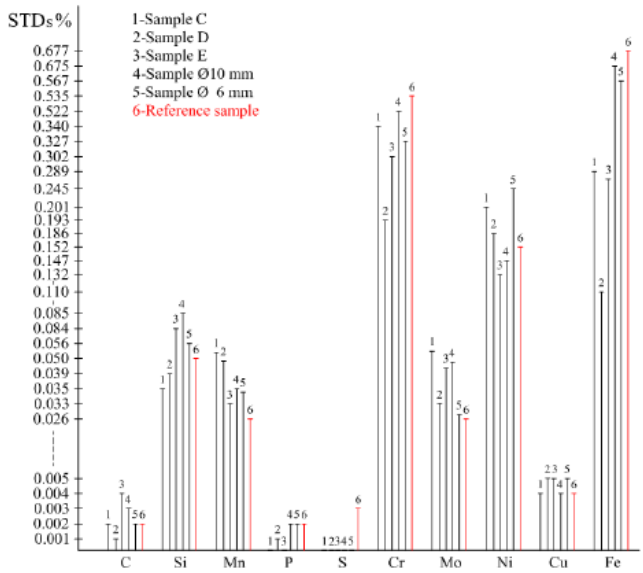

Figure 3. The standard deviation values for all samples.

The microstructure of samples was investigated by a REICHERT optical microscope equipped with an automatic line for image acquisition and processing. The SEM analysis were done with a XL-30-ESEM TMP microscope equipped with ED-XRF spectrometer (Energy Dispersive X-ray Fluorescence) Buhler and MLG 11 equipments were used for specific sample surface finishing needed for microscopical investigations and for OES-ASE analysis.

The samples from Ti6Al4V are samples taken from medical devices of millimeter size, used for medical implants and non-invasive interventions (cell manipulation). Their characterization was performed by electronic microscopy using the JEOL scanning electron microscope in the laboratory at the FEMTO-ST Besançon Institute in France, to highlight the nanometric dimensions of Ti6Al4V powders.

Surface micro-geometry topography was studied by atomic force microscopy (AFM). To investigate the characteristics and surface quality of these materials the atomic force microscope type NTGRA Probe NanoLaboratory NT-MDT from the INCDMTM Institute in Bucharest was used. The AFM investigation procedure consisted in identifying and photographing damaged areas on the surface of a medical device made of Ti6Al4V, where 50 x 50 μm areas were selected. Surface topography analysis was performed for each area and the topographic parameters were determined using the NOVA SPM Software - the microscope software. The prosthetic elements studied from the Ti6Al4V alloy were made by Rapid Prototyping (RP) technology. The analyzed sample was obtained by rapid prototyping on the EOSINT M270 / PSW3.4 laser sintering machine from the National Institute for Research and Development for Mechatronics and Measurement Engineering (INCDMTM) in Bucharest. The prototyping machine performs the piece by depositing successive layers of powder starting from a basal plane. Each deposited layer is fixed to the previous layer by sweeping with a laser beam that performs sintering, "melting" the powder particles.The alloy in the form of powder are melted directly with a laser beam and created layer by layer a solid, three-dimensional object. This technology offers adaptation possibilities for patients requiring any type of implant.

Table 1. Results for 316L samples tested spectrochemically.

Elements	**C**	**Si**	**Mn**	**P**	**S**	**Cr**	**Mo**	**Ni**	**Al**	**Co**	**Cu**	**Nb**	**Ti**	**V**	**W**	**B**	**Ca**	**Fe**
Sample C	0.041	1.46	1.95	0.015	0.002	17.77	2.31	12.71	0.07	0.11	0.03	0.04	0.021	0.09	0.26	0	0	63.11
	0.045	1.50	1.83	0.015	0.002	17.76	2.27	12.49	0.07	0.10	0.03	0.04	0.016	0.09	0.25	0	0	63.48
	0.045	1.43	1.94	0.015	0.002	17.35	2.37	12.98	0.09	0.21	0.04	0.03	0.020	0.07	0.42	0	0	62.99
	0.045	1.43	1.94	0.015	0.002	17.35	2.37	12.96	0.09	0.21	0.03	0.03	0.020	0.07	0.42	0	0	63.15
	0.040	1.50	1.87	0.014	0.002	18.16	2.26	12.77	0.08	0.14	0.03	0.05	0.020	0.10	0.30	0	0	62.68
Cmed (%)	0.043	1.46	1.91	0.015	0.002	17.68	2.32	12.78	0.08	0.15	0.03	0.04	0.019	0.08	0.33	0.00	0.00	63.08
STDs	0.002	0.035	0.053	0.000	0.000	0.340	0.053	0.201	0.010	0.053	0.004	0.008	0.002	0.013	0.084	0.000	0.000	0.289
U(95%)	0.006	0.070	0.106	0.003	0.003	0.680	0.105	0.402	0.020	0.106	0.009	0.017	0.005	0.027	0.169	0.003	0.003	0.578
Elements	**C**	**Si**	**Mn**	**P**	**S**	**Cr**	**Mo**	**Ni**	**Al**	**Co**	**Cu**	**Nb**	**Ti**	**V**	**W**	**B**	**Ca**	**Fe**
Sample D	0.042	1.49	1.86	0.015	0.002	17.75	2.32	12.82	0.08	0.14	0.04	0.04	0.018	0.09	0.32	0	0.001	62.98
	0.043	1.52	1.98	0.016	0.002	17.45	2.29	12.63	0.08	0.15	0.03	0.05	0.021	0.08	0.44	0	0	63.09
	0.043	1.52	1.98	0.016	0.002	17.45	2.29	13.09	0.08	0.15	0.04	0.05	0.021	0.08	0.32	0	0	62.88
	0.041	1.46	1.95	0.015	0.002	17.77	2.31	12.71	0.07	0.11	0.03	0.04	0.021	0.09	0.26	0	0	63.11
	0.045	1.43	1.94	0.015	0.002	17.35	2.37	12.96	0.09	0.21	0.03	0.03	0.020	0.07	0.42	0	0	63.15
Cmed (%)	0.043	1.48	1.94	0.015	0.002	17.55	2.32	12.84	0.08	0.15	0.03	0.04	0.020	0.08	0.35	0.00	0.00	63.04
STDs	0.001	0.039	0.049	0.001	0.000	0.193	0.033	0.186	0.007	0.036	0.005	0.008	0.001	0.008	0.076	0.000	0.000	0.110
U(95%)	0.004	0.078	0.098	0.003	0.003	0.385	0.066	0.372	0.014	0.073	0.011	0.017	0.004	0.017	0.151	0.003	0.003	0.221
Elements	**C**	**Si**	**Mn**	**P**	**S**	**Cr**	**Mo**	**Ni**	**Al**	**Co**	**Cu**	**Nb**	**Ti**	**V**	**W**	**B**	**Ca**	**Fe**
Sample E	0.042	1.51	1.87	0.015	0.002	17.83	2.26	12.68	0.07	0.12	0.04	0.04	0.021	0.08	0.25	0	0	63.17
	0.042	1.63	1.92	0.015	0.002	17.44	2.34	12.71	0.07	0.12	0.03	0.04	0.020	0.08	0.30	0	0	63.23
	0.051	1.46	1.88	0.015	0.002	16.99	2.35	12.65	0.10	0.23	0.04	0.03	0.020	0.07	0.45	0	0	63.67
	0.044	1.43	1.94	0.014	0.002	17.50	2.32	12.78	0.10	0.21	0.03	0.03	0.017	0.07	0.44	0	0	63.07
	0.045	1.43	1.94	0.015	0.002	17.35	2.37	12.98	0.09	0.21	0.04	0.03	0.020	0.07	0.42	0	0	62.99
Cmed (%)	0.047	1.44	1.92	0.015	0.002	17.28	2.35	12.80	0.10	0.22	0.04	0.03	0.019	0.07	0.44	0.00	0.00	63.24
STDs	0.004	0.084	0.033	0.000	0.000	0.302	0.042	0.132	0.015	0.054	0.005	0.005	0.002	0.005	0.091	0.000	0.000	0.265
U(95%)	0.008	0.168	0.066	0.003	0.003	0.604	0.084	0.164	0.030	0.107	0.011	0.011	0.004	0.011	0.182	0.003	0.003	0.529
Elements	**C**	**Si**	**Mn**	**P**	**S**	**Cr**	**Mo**	**Ni**	**Al**	**Co**	**Cu**	**Nb**	**Ti**	**V**	**W**	**B**	**Ca**	**Fe**
Sample Φ 10 mm	0.031	1.40	1.90	0.016	0.002	17.58	2.38	12.70	0.07	0.13	0.03	0.03	0.018	0.08	0.32	0.001	0	63.29
	0.028	1.52	1.97	0.017	0.002	18.68	2.36	12.92	0.07	0.13	0.03	0.04	0.022	0.08	0.30	0	0	61.81
	0.030	1.64	1.94	0.015	0.002	17.59	2.29	12.55	0.08	0.12	0.03	0.04	0.019	0.09	0.24	0	0.001	63.31
	0.034	1.54	1.90	0.020	0.002	17.57	2.27	12.61	0.08	0.13	0.03	0.05	0.017	0.09	0.27	0	0	63.38
	0.026	1.52	1.97	0.015	0.002	17.38	2.32	12.79	0.07	0.13	0.04	0.04	0.020	0.08	0.29	0	0	63.29
Cmed (%)	0.030	1.52	1.94	0.017	0.002	17.76	2.32	12.71	0.07	0.13	0.03	0.04	0.019	0.08	0.28	0	0.00	63.02
STDs	0.003	0.085	0.035	0.002	0.000	0.522	0.046	0.147	0.005	0.004	0.004	0.007	0.002	0.005	0.030	0.000	0.000	0.675
U(95%)	0.007	0.171	0.070	0.005	0.003	1.044	0.092	0.293	0.011	0.009	0.009	0.014	0.005	0.011	0.061	0.003	0.003	1.350

3. RESULTS

The results of the 316L steel samples tested spectrochimically are presented into Figs. 2 and 3, and Table 1. Each sparking area of the 316L specimen tested spectrochimically was visually examined, after which images from the morphologically different areas were acquired. Thus, overall images will be presented. After analyzing the images acquired for each sparking area, the most representative images were selected, which are presented in the following.

MICROSTRUCTURAL ANALYSIS FOR 316L ALLOY BY OPTICAL MICROSCOPY.

Figure 4.a) Overall image of the sparking area.

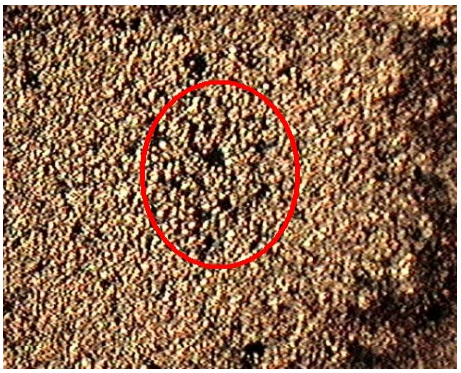

Figure 4.b) Detail.

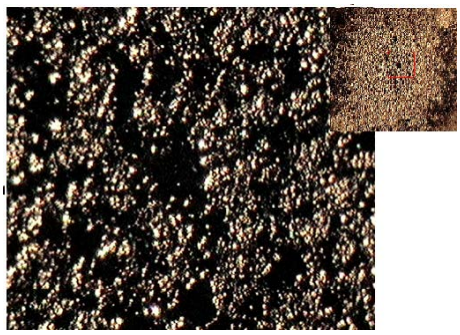

Figure 5. Morphological aspects of a sparking surface, central area of a sparking surface

Figure 6. Morphological aspects of a sparking surface; marginal area of a sparking surface.

MICROSTRUCTURAL ANALYSIS FOR 316L ALLOY BY SEM-EDS MICROSCOPY

The overall image of the sparking surface obtained in the SE (Secondary Electrons) mode and the image obtained in BSE (Backscattered Electron) mode is shown in Fig.7 a,b). The images obtained in the BSE mode aim to reveal changes in chemical homogeneity in the target area.

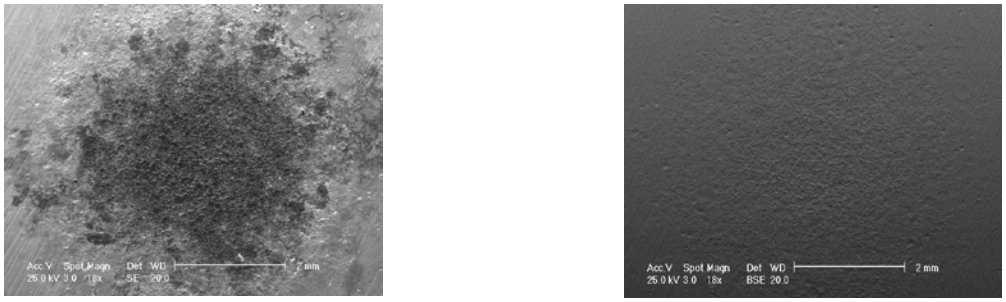

Figure 7. a). SE mode image of the sparking surface; b). BSE mode image of the sparking surface.

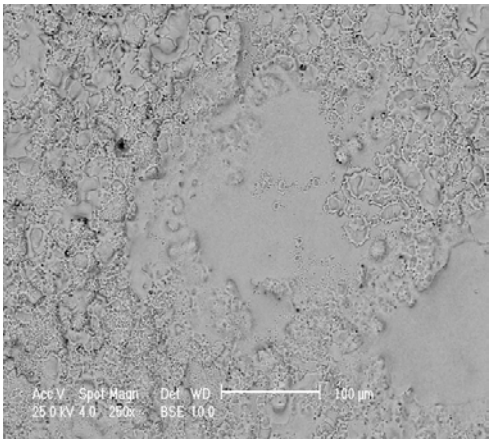

Figure 8. BSE image, overall, sparking surface, peripheral area, 250X magnification.

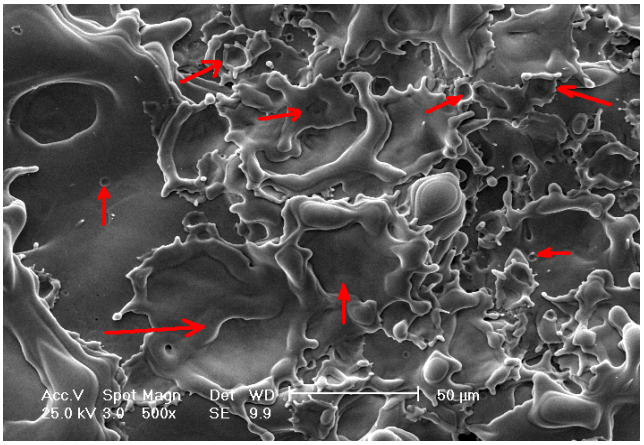

Figure 9. Overall image of the sparking surface, 500X magnification.

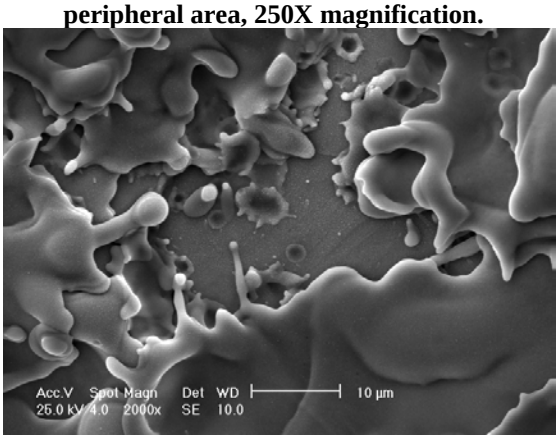

Figure10. Image in SE mode (detail) of the sparking surface, median area, 2000X magnification.

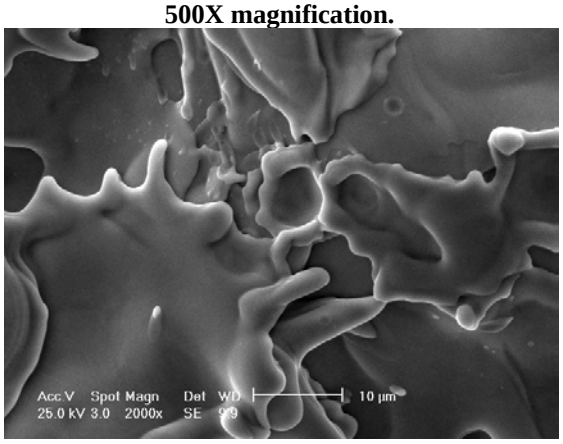

Figure 11. Image in SE mode (detail) of the sparking surface, central area, 2000X magnification.

ED-XRF analysis (Energy Dispersive X-ray Fluorescence) can be correlated with investigations BSE (backscattered electrons) to estimate the combined effect of composition-segregation, or distillation of elements in sparking surface. Therefore, it was decided that the areas investigated by SEM to be analyzed through ED-XRF. Thus, Fig. 12 a),b) shows the emission of characteristic spectrum from X-ray induced by the incident electron beam.

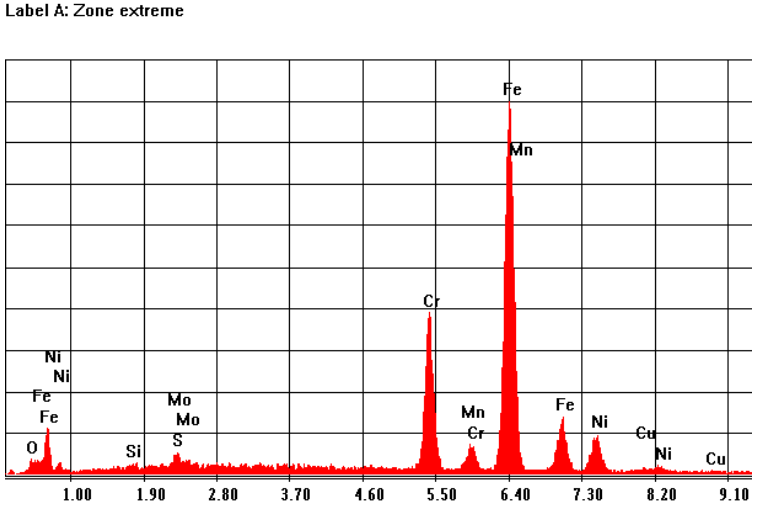

Figure 12 a). ED-XRF spectrum achieved for sparking surface-zone extreme/ peripheral.

Extremity	
Element	C (%)
Cr	17.48
Ni	9.99
Mo	2.68
Mn	1.22
Si	0.53
Cu	1.64
O	2.94
S	0
Fe	63.52
Total	100

Figure 12 b). Mass concentrations corresponding for Fig.12a.

MICROSTRUCTURAL ANALYSIS OF TI6AL4V TITANIUM ALLOY BY SEM ANALYSIS

For a more accurate presentation of the morphology of the Ti6Al4V powders of the analyzed structures, several electron microscopy images, obtained for the most varied areas of the analyzed sample, will be presented. To investigate the characteristics and surface quality of these materials, microscopic and profile analysis was performed.

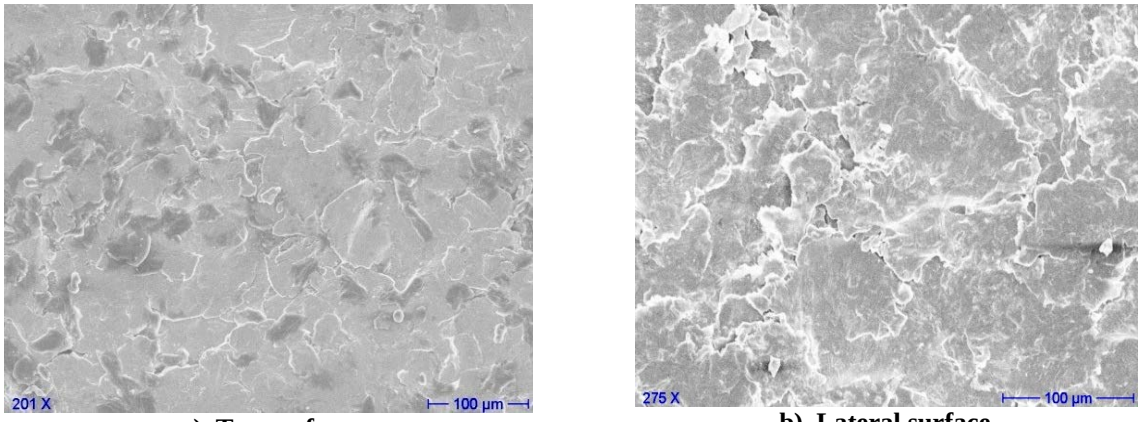

a). Top surface **b). Lateral surface**

Figure13. SEM micrograph of Ti6Al4V part

THE GEOMETRY MICRO-TOPOGRAPHY STUDY BY ATOMIC FORCE MICROSCOPY (AFM)

Based on the surfaces identified by the CCD camera of the AFM microscope, several areas of damaged areas of the prosthetic elements were selected, as shown in Fig. 14. In these areas the AFM topographic analysis was performed at nanometric level.

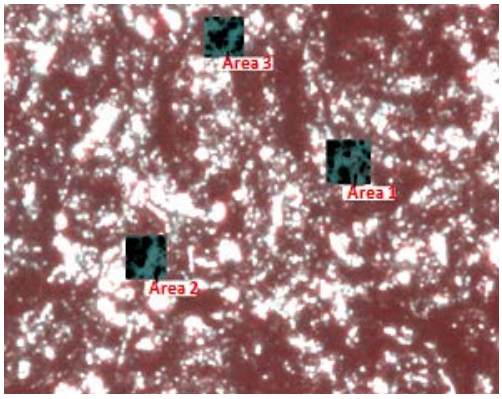

Figure 14. Areas selected for topographic analysis.

In the images below (Figs.15-17) presents the results of the analysis,with AFM for selected areas. In all these images show that: the surface of the 2D scan of each zone (a), converted into 3D scanned surface (b) determined topographic parameters (c), the average profile in the x direction (d) and the average profile in the y direction (e).

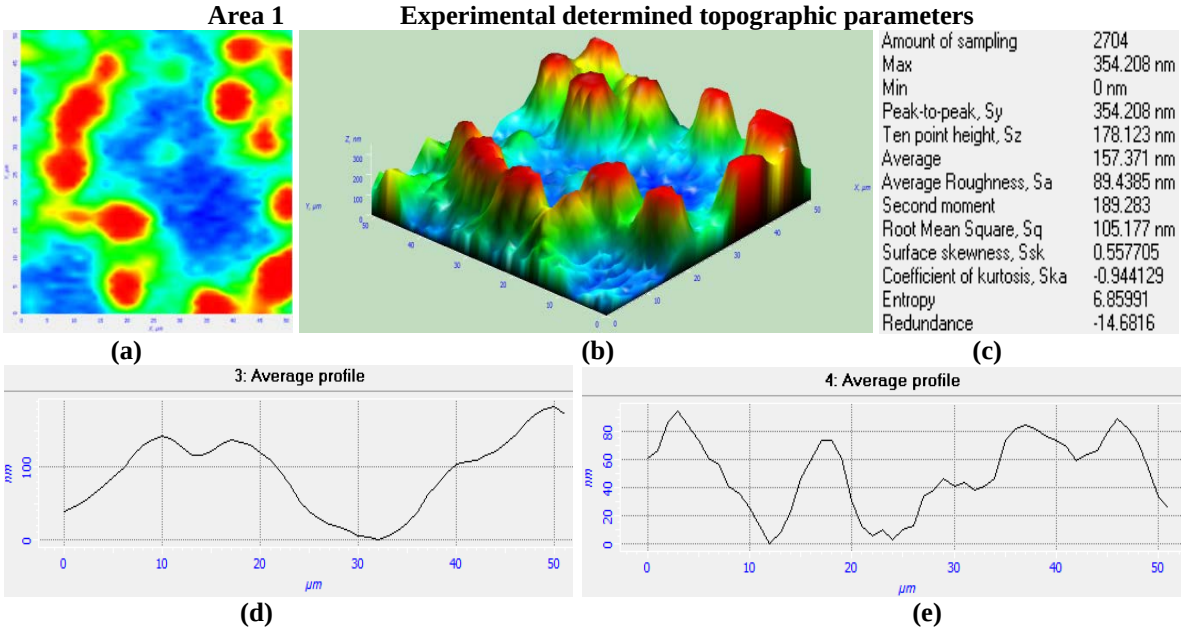

Figure 15. AFM analysis of surface area 1:
(a) 2D scanned surface, (b) converted to 3D scanned surface, (c) determine topographic parameters, (d) The average profile in the x direction, (e) The average profile in the y-direction.

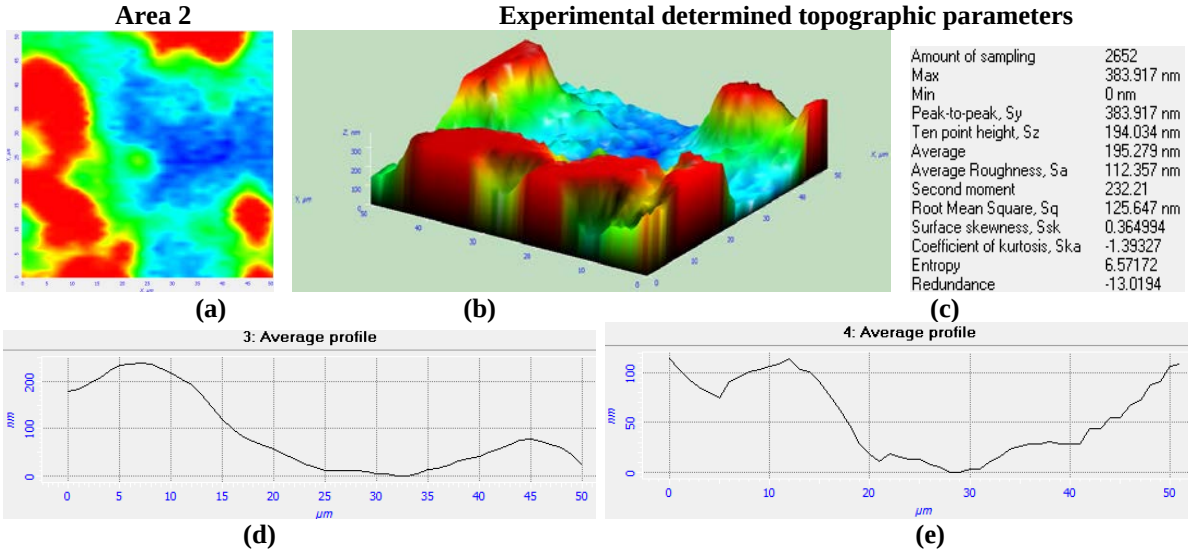

Figure 16. AFM analysis of surface area 2:
(A) 2D scanned surface, (b) converted to 3D scanned surface, (c) determine topographic parameters, (d) The average profile in the x direction, (e) The average profile in the y-direction.

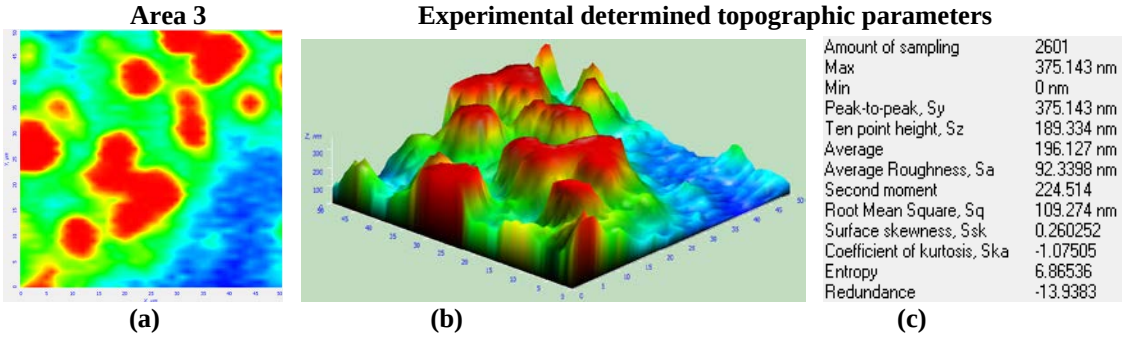

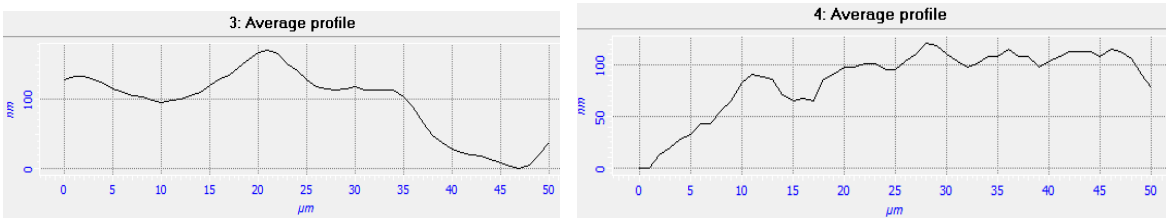

(d) **(e)**

Fig.17. AFM analysis of surface area 3:
(A) 2D scanned surface, (b) converted to 3D scanned surface, (c) determine topographic parameters, (d) The average profile in the x direction, (e) The average profile in the y-direction

Syntheses of experimental research are presented in Table 1: experimentally determined values of the main topographic parameters and their average value calculated for areas of Ti6Al4V non-polished samples.

Table 1. Topographic values of the main parameters experimentally determined and their average value calculated for the Ti6Al4V non-polished samples.

Area of non-polished samples	R_a (nm)	h_{max} (nm)	S_{sk}	S_{ka}
Area 1	89.438	354.208	0.557	-0.944
Area 2	112.357	383.914	0.364	-1.393
Area 3	92.339	375.143	0.260	-1.075
Average calculated value	**98.044**	**371.088**	**0.394**	**-1.137**

Subsequently, the parts of the prosthetic components were polished to compare the roughness of the surfaces with those of the non-polished samples. A synthesis of experimental results is presented in Table 2: experimentally determined values of the main topographic parameters and their average value calculated for areas of Ti6Al4V polished samples.

Table 2. Topographic values of the main parameters experimentally determined and their average value calculated for the Ti6Al4V polished samples.

Area of polished samples	R_a (nm)	h_{max} (nm)	S_{sk}	S_{ka}
Area 1	79.785	297.592	0.469	-0.876
Area 2	105.453	304.356	0.342	-1.269
Area 3	89.67	343.541	0.253	-0.925
Average calculated value	**91.636**	**315.163**	**0.354**	**-1.023**

4. DISCUSSIONS

Knowing the exact chemical composition as a biocompatible metal material is a major requirement for estimating an implant composition. In this regard the conformity requirements for biocompatible steels 316L are specified in the ISO 5832-1/1999 standard. Determination of carbon content in special-purpose steels (316L) should be rigorously accurate because their biocompatibility decreases drastically if they contain more than 0.03% C. Comparing the values of the carbon concentrations in the samples C, D, E (see supplementary information in Online Resource 1) with the values stipulated in SR ISO 5832-1 result that they do not satisfy the conditions imposed by the standard. Concentrations from the 3 samples, of other 316L alloy elements such as nickel, sulfur, chromium, phosphorus, etc. are in accordance with the requirements of standard 5832-1 / 1999. However, even if the carbon framing is considered to be at the lower limit of the confidence interval, the samples

can not be considered biocompatible. Concentrations of elements in the sample of Φ = 10 mm are comprehensively covered by SR ISO 5832-1. However, framing the sample Φ = 10 mm as biocompatible is risky because the real carbon concentration is in the range [0.23 ÷ 0.37] with a uncertainty of 95%. So, it is every bit as likely that the carbon concentration was greater than 0.03%, in this case, it is risky to consider that the material is biocompatible. Therefore, assurance of compositional compliance must be one of the rigorously satisfied requirements in choosing a material for use in biomedical applications. The achievement of this requirement for biocompatible implants must be respected in order to reduce the risk of malpractice in medical practice.

In Figs. 5 and 6 (a, b) are presented the morphological aspects of a sparking surface at a scale of tenths of millimeters. Figure 4 shows a specific attack mode of the argon discharge channels, during specimen sparking for spectrochemical analysis, respectively a pitting attack in the center of the sparking zone. Thus, about 15 pores (excavations) can be counted in the circle with a radius of about 30% of the radius of the sparked area (Fig. 5). On the right side you can see the characteristic aspect of the border, with the crevices of attack, but with less incidence of pitting. The detail of the central area in Fig. 4 reveals the superficial morphology of the crevasses and Fig. 5 reveals the cylindrical morphology of the crevasses surrounding the central crevasse. On the other hand, Figs. 4-6 it is noticed that there is no local area that has not been bombarded / sparked. The justification would be that there are no traces of morphological aspects generated by sample preparation, as seen at the periphery of the whole picture. The image in Fig. 6 reveals the existence of concentrated attack zones at the periphery of the sparked area and the lack of an attacking, sparking”texture”. The images of the peripheral areas of the sparked area reveal the scattering sparks and the existence of the crevices in a”fully attacked field”, but with a lower intensity. Optical microscopy investigations revealed several new aspects for the spectral analysis of 316L steels, respectively: the sparked area is attacked relatively uniformly on 85-90% of the apparent spark gap diameter; at the periphery of the spark spot there is a sudden transition from the uniform attack regime to unattached areas; inclusions and other defects are preferential attack points of sparks and are the cause of the generation of pitting and crevices in the sparking area; it has been estimated that a spark (a discharge channel) "attacks" an area of about 300 mm^2; some general images suggest a non-homogeneous attack caused by the specific distribution of the sparking channels.

Images obtained with retroreflected electrons are intended to highlight the non-homogeneous chemical composition of the target area. The picture in Fig. 7b) aimed at highlighting possible changes in the distribution of chemical elements in the sparking area. This figure does not reveal significant inhomogeneities of the chemical composition, but only shows the diminution of the morphological differences due to the mode of obtaining the SEM image. From Fig. 7, the morphology of the spark fingerprint is very clear, namely, it is formed by an approximately circular central area where the incidence of individual sparks has destroyed the pre-existing structure. This area has a diameter of about 2 mm. Circumcised on this disc there is a crown with a side of about 1 mm in which the incidence of spark bombardment is reduced, but in this crown there are recesses (pitting or crevices) whose genesis can most likely be attributed to the discharge channels ”fixed”. Fixing these discharge channels in certain areas remains a subject to be researched. From the analysis Fig. 9 it is noticed that arrow-marked craters have diameters of about 4 μm. The image also reveals large craters that have most likely been formed by repeated bombardment of those areas. The phenomenon is known as spark fixation. Large craters, which are well individualized, have diameters of 35 μm, 40 μm. After the Argon ion “bombardment” resulted”molten metal waves” and even droplets of ellipsoidal form, which are chained in a complex way. The BSE image of Fig. 8 reveals combined, morphological and compositional aspects in the peripheral

region. From a morphological point of view, Fig. 8 better reveals the propagation of the shock wave leading to the formation of craters collars, with dimensions larger than 10 μm. Also, Fig. 8 clearly reveals the presence of pittings that were not covered by the melts. There seem to have been inclusions there, which were massively attacked and excavated in depth. The image in Fig. 8 brings to the examiner's attention the idea of shock wave generated at the impact of the ion formation / atoms occurring on the surface of the sample.The median image, obtained at a magnification of about 2000x (Fig. 10), shows in the central area, light traces of particles embedded in the melt, about 70-85% of the particle volume. The image of the same area, taken at a magnification of 2000x (Fig. 11), gives the real surface morphology. The images in Figs. 10-11, as well as the other images presented, undoubtedly highlights the explosive nature of individual craters. All experimental evidence, optical microscopy and electron microscopy, lead to the idea of a local discharge. The discharges are made through by "channels" with relatively large diameters, larger than 2 μm, which remains an aspect to be explained. The topographic parameters determined by the atomic force microscopy (see Figs. 14-17) study for the Ti6Al4V alloy sample (e.g. the average roughness Sa, the maximum height hmax, the Ssk surface asymmetry, the Ska flattening coefficient) provide information on the surface areas of the parts. The Ssk asymmetry index measures the degree of asymmetry of a distribution and, along with the Ska flattening index, characterizes the distribution. The Ssk asymmetry index is negative or positive, as the survey is asymmetric to the left or right. A symmetric distribution, such as normal distribution, has a null asymmetry. The Ska flattening coefficient is part of the indices of appreciation of the shape of a distribution. A large flattening index shows a large "queue" distribution (there are distant averages), while a low flattening index shows a distribution in which fewer categories are deviated from the mean. In the case of a distribution close to the normal distribution, the coefficient of flattening is around 3.

For the Ti6Al4V sample, with respect to the values of the Ssk asymmetry index, it has low values, Sskm = 0.394 < 1 and Sskm = 0.354 < 1 (for polished sample), indicating a distribution very close to symmetry. The negative values of the Ska flattening coefficient indicate a platictic reputation (the curve is flattened), Ska = -1.137, respectively Ska= -1.023 (for polished sample). As roughness is small, the surface is smoother, more suitable for further use in certain biomedical applications. From the experimental study conducted by investigation type SEM carried out on samples of Ti6Al4V alloy it can reveal that surface topography of the devices obtained by the selective laser sintering process is more uniform than that of the pieces obtained by conventional processing technologies.

5. CONCLUSIONS

During the last decades, considerable attention has been directed towards the use of bioactive implants fixation. Fixing bioactive it is defined by the interfacial binding an implant for a human tissue.Type of material, manufacturing process, chemical composition, mechanical properties and processing conditions significantly influence the interaction between material and bone tissues. Implant surface has decisive influence in fixing and adhesion living tissue to it. With increasing roughness surface of implant, increases the adherence living tissue and increase pull off strength of due to specific surface larger of the implant in tissue-implant contact area. In the case of biomedical applications, the influence of surface roughness on the rate of fixing biomechanics of the implants from hard tissue is a key factor. Also metallurgical parameters correlated with the chemical composition of the sample material are an important criterion for biocompatibility that it must fulfill prosthetic devices.

The most important aspect, for the alloy steel samples revealed by metallographic microscopy is rough granular appearance (the crevasse) of the center sparked area in relation to adjacent areas. On the other hand, observing with the naked eye of sparks, suggests that the marginal areas of the sparked area are rough. This roughness aspect may be beneficial for the realization of potential biocompatible interfaces, layer-substrate metal, suitable for ceramic coatings on metal substrates. Another important aspect emerging from studies on 316L steel alloys is that the OES-ASE spectrometry method could be used for architecturized the metal surfaces in order to obtain porous surfaces with controlled properties favorable to bioactive deposits. By analyzing detail images by SEM microscopy, the areas from inside sparked area (Figs. 7-11) we may conclude that these images do not reveal significant inhomogeneity of the alloy chemical composition for the steel samples. After the investigations carried out on Ti6Al4V alloy samples via atomic force microscopy AFM, was observed significant variation in both types of surface roughness and can mention the following conclusions: surface grinding pieces is proven primarily by the fact that hmax decreases from averages of 371.088 nm to the average values of 315.163 nm (as a result of the removal of polishing material on the initial surface obtained after the laser sintering process); R_a decreases also along with processing from the average values of Ra = 98.044 nm to the average values of R_a = 91.636 nm, surfaces become smoother, with less roughness.

Thus, after polishing, the surface roughness decrease, the surface is more smooth, more suitable for further use in biomedical applications which require satisfaction of these properties, such as cardiovascular implants (stent), devices for micromanipulation of cells, etc.

From the studies made it can be said that the Ti6Al4V alloy implants obtained by SLS technologies have a major advantage, related to the special geometric form for medicine, these technologies favoring the creation of a personalized implant for each patient. As regards the quality of materials (Ti6Al4V alloys), for various prosthetic elements and implants, it is much improved.

In the context of intensifying research on the development of various components and medical prostheses, this paper confirms that the choice of materials and appropriate manufacturing technologies involves a thorough study and is a key factor in their realization.

Acknowledgements: *Authors thank to colleagues from INCDMTM Institute from Bucharest for the selective laser sintering tests, FEMTO-ST Institute from Besancon for the material characterisation facilities, and Politehnica University of Bucharest and LISEOFRX laboratory of UPB Bucharest for the material characterisation facilities.*

REFERENCES

[1] Manivasagam, G., et al., *Recent Patents on Corrosion Science*, **2**, 40, 2010.
[2] Sivakumar, M, et al., *J. Mater. Sci*., **13**, 142, 1994.
[3] Weldon, L.M., et al., *J. Mate. Sci.: Materials in Medicine*, **16**, 107, 2005.
[4] Shih, C., et al., *J. Biomed. Mat. Res.*, **52**, 323, 2000.
[5] Bertrand, O.F., et al., *J. Am. Coll. Cardiol.*, **32**, 562, 1998.
[6] Palmaz, J.C., *Texas Heart Inst. J*., **24**, 156, 1997.
[7] Dong, H., et al., *J. Mater. Sci. Mat in Med*., **28**(1), 5, 2017.
[8] Beddoes, J., Bucci, K., *J. Mater. Sci. Mat in Med*., **10**, 389, 1999.
[9] Williams, D.F., *Current perspectives on implantable devices*, India: Jai Press, 1990.
[10] Amel-Farzad, H., et al., *Eng Fail Anal*, **14**, 1205, 2007.

[11] Mudali, K.U., et al., *Corrosion of bio implants. Sadhama*, **28**(3-4), 601, 2003.
[12] Bandyopadhyay, A., et al., *Acta Biomater*, **6**(4), 1640, 2010.
[13] Sachiko, H., et al., *Biomaterials*, **26**, 4912, 2005.
[14] Manivasagam, G., et al., *Corrosion Rev.*, **21**, 125, 2003.
[15] Gheorghe, G., et al., *Digest J. of Nanomaterials and Biostructures*, **8**(3), 1037, 2013.
[16] Elias, C.N., et al., *Biological Materials Science*, **2008**, 46, 2008.
[17] Geetha, M., et al., *Prog Mater Sci.*, **54**, 397, 2009.
[18] Hoeppner, D.W., Chandrasekaran, V., *Wear*, **173**, 189, 1994.
[19] Hsu, S.H., et al., *Bio Med Mater Eng*, **17**, 53, 2007.
[20] Yue, T.M., et al., *Mater Lett*, **52**(3), 206, 2002.
[21] Liping, L., Patent 022887 - *Nanocoating for improving biocompatibility of medical implants*, 2006.
[22] Kappelt, G., Kurze, P., Banerjee, D., Patent 0243242 - *Method for producing a corrosion-inhibiting coating on an implant made of a biocorrodible magnesium alloy and implant produced according to the method*, 2008.
[23] Deutchman, A.H., Partyka, R.J., Borel, R.J., Patent 0221683 - *Orthopaedic implants having self-lubricated articulating surfaces designed to reduce wear, corrosion, and ion leaching*, 2008.
[24] Basu, J., et al., *Appl. Phys. Lett.*, **94**, 171114, 2009.
[25] Bonfield, W., et al., *Acta Materialia*, **46**, 2509, 1998.
[26] Karen, N., *Stress corrosion cracking in biomedical (metallic) implants Titanium-Nickel (TiNi) alloy*, Cordis – NDC, 2003.
[27] Corrosion Source, Available from *http://www.corrosionsource.com/technicallibrary/corrdoctors/Modules/Implants/Websites.html*, 2000.
[28] Aksakal, B., et al., *J. Fail Anal Prev*, **4**(3), 17, 2004.
[29] Anghelina, F.V., et al., *Applied Surface Science*, **285**, 65, 2013.
[30] Norton, M.G., et al., *Appl. Phys. Lett.*, **56**, 2246, 1990.
[31] Despa, V., et al., *The study of materials used to manufacture prosthetic components for medical implants*, 10th International Conference on Materials Science & Engineering, Transilvania University of Brasov, Romania, 2017.
[32] Barbes, L., et al., *Romanian Reports in Physics*, **66**(3), 765, 2014.
[33] Ionita, I., et al., *Journal of Optoelectronics and Advanced Materials*, **10**(11), 2859, 2008.
[34] Ionita, I., et al., *Revista de Chimie*, **64**(6), 612, 2013.
[35] Radulescu, C., et al., *Journal of Science and Arts*, **1**(34), 77, 2016.
[36] Poinescu, A.A., et al., *Revista de Chimie*, **65**(10), 1245, 2014.
[37] Sencovici, M., Pehoiu, G., Ecology, Economics, Education and Legislation Conference Proceedings, *International Multidisciplinary Scientific GeoConference-SGEM*, **I**, 277, 2016.
[38] Pehoiu, G., Frinculeasa, M.N., *Economics, Education and Legislation Conference Proceedings, International Multidisciplinary Scientific GeoConference-SGEM*, **I**, 735, 2015.
[39] Ispas, S., Pehoiu, G., Simion, T., *Economics, Education and Legislation Conference Proceedings, International Multidisciplinary Scientific GeoConference-SGEM*, **II**, 1055, 2011.
[40] Murarescu, O., Pehoiu, G., et al., *Political Sciences, Law, Finance, Economics and Tourism, International Multidisciplinary Scientific Conferences on Social Sciences and Arts*, **IV**, 59, 2014.